Analysis and Design of Microslab Waveguide

BRIAN YOUNG AND TATSUO ITOH, FELLOW, IEEE

Abstract — **Microslab[1], a novel low-loss semiplanar waveguide, is studied to provide design charts for the propagation constant and characteristic impedance. A parallel-plate analysis is performed to provide design guidelines based on frequency, conductor loss, and size. A mode-matching procedure is then used to build the design charts. Results are provided for Microslab implementation on GaAs substrates.**

I. Introduction

MICROSLAB[1] waveguide was recently proposed to address the problem of conductor losses in millimeter-wave waveguides [1]. Microslab uses a microstrip-like geometry with insulating dielectrics to reduce the ohmic losses in the conductors (see Fig. 1). Although the metallization on the center strip is not required for wave guidance, it is retained to provide improved binding of the wave and to lower dispersion. It is in this respect that Microslab differs from other mm-wave dielectric insulated waveguides [2], [3].

In order to design components in Microslab, information of engineering utility is required for the loss, propagation constant, and characteristic impedance of the dominant mode [4] along with the propagation constant of the first higher order mode. Useful results to date include only an approximate closed-form formula for the impedance [5].

This paper presents the information necessary to design Microslab lines on GaAs substrates by using a mode-matching analysis to construct design charts. Mode matching is a very computationally intensive solution technique which becomes even more so for complicated structures. Numerical optimization to minimize the conductor loss is not feasible. To reduce the problem, a thin-strip approximation will be used; however, this approximation precludes the calculation of the conductor loss [6]. In order to design Microslab structures for minimum conductor loss, the parallel-plate waveguide is analyzed for the conductor loss and optimized to provide design charts from which Microslab dimensions can be chosen. In this way, the loss is optimized in an approximate manner while reducing the computional load of the mode-matching analysis. With these dimensions, the mode-matching analysis is applied for several strip widths to build design charts for the propagation constant and characteristic impedance.

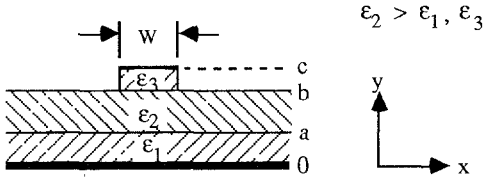

Fig. 1. Microslab waveguide.

The paper is divided into the following sections. The parallel-plate waveguide analysis is presented in Section II. The mode-matching formulation and characteristic impedance definition appear in Section III. In Section IV, design tradeoffs derived from the parallel-plate and mode-matching analysis are discussed. The design charts for GaAs substrates appear in Section V along with some representative field plots. Since Microslab is intended for mm-wave operation in low-loss monolithic components, design charts are provided for GaAs substrates only. Section VI concludes the paper.

II. Parallel-Plate Analysis

For high frequencies and/or wide strips, Microslab operation is similar to the dielectric layered parallel-plate waveguide shown in Fig. 2. Conductor losses can be reduced by reducing the tangential magnetic field strength at the conductors. For the structure in Fig. 2, this can be accomplished by selecting $\epsilon_2 > \epsilon_1, \epsilon_3$ and operating the waveguide at a frequency such that $(\beta/\beta_0)^2 > \epsilon_1, \epsilon_3$, which will induce decaying fields in the ϵ_1 and ϵ_3 layers. Increasing the frequency further reduces the loss due to the increased decay rate in the fields. However, it is well known that for such structures the dominant mode switches types from TM^y at low frequencies to TE^y at high frequencies [7], [8]. The physical reason for this phenomenon is that TM^y operation is induced at low frequencies by the presence of two conductors. At high frequencies, the fields decay and do not see the conductors, resulting in an asymmetric slab as the effective waveguide, for which the dominant mode is always TE^y [9]. Therefore, the dispersion curves for the two modes must cross at some frequency, f_s. Since operation in the TE^y mode is undesirable due to the unfavorable field configuration, the operation frequency is bounded above by f_s, where the loss is mini-

Manuscript received February 5, 1987; revised May 4, 1987 This work was supported in part by a grant from Martin Marietta Laboratories.

The authors are with the Department of Electrical and Computer Engineering, University of Texas at Austin, Austin, TX 78712.

IEEE Log Number 8715668.

[1] Microslab is a trademark of the Martin Marietta Corporation.

0018-9480/87/0900-0850$01.00 ©1987 IEEE

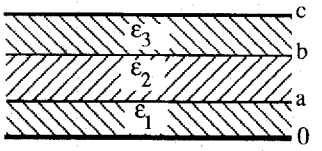

Fig. 2. Parallel-plate waveguide model for Microslab.

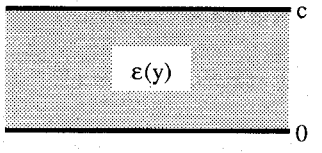

Fig. 3. Generalized parallel-plate waveguide.

mum. For Microslab, the E_{11}^{y} mode is dominant at low frequencies, and the E_{11}^{x} is dominant at high frequencies.

Both the parallel-plate optimization and the mode-matching analysis require the calculation of the modes of the parallel-plate waveguide. In order to simplify the notation, we will begin with the general waveguide of Fig. 3, where $\epsilon(y)$ is stratified in the y direction. The fields can be generally described in terms of scalar potentials [10] as

$$\boldsymbol{H} = \nabla \times \left[\theta(x)\phi(y)e^{-jk_z z}\hat{\boldsymbol{y}}\right] \tag{1}$$

for the TM^{y} modes and

$$\boldsymbol{E} = -\nabla \times \left[\bar{\theta}(x)\bar{\phi}(y)e^{-jk_z z}\hat{\boldsymbol{y}}\right] \tag{2}$$

for the TE^{y} modes. An overbar differentiates between TE^{y} and TM^{y} quantities, and vectors are in boldface italic type. Application of (1) and (2) with the appropriate boundary conditions yields the eigenvalue equations for the guided modes.

For the waveguide of Fig. 2, $\theta(x) = \bar{\theta}(x) = 1$. The TM^{y} and TE^{y} eigenvalue equations are, respectively,

$$\begin{aligned}&(k_{1y}/\epsilon_1)\tan(k_{1y}a) + (k_{2y}/\epsilon_2)\\ &\quad\cdot\tan\left[k_{2y}(b-a)\right] + (k_{3y}/\epsilon_3)\tan\left[k_{3y}(c-b)\right]\\ &= (k_{1y}/\epsilon_1)\tan(k_{1y}a)(\epsilon_2/k_{2y})\\ &\quad\cdot\tan\left[k_{2y}(b-a)\right](k_{3y}/\epsilon_3)\tan\left[k_{3y}(c-b)\right]\end{aligned} \tag{3}$$

where $\omega^2\mu_0\epsilon_1 = k_z^2 + k_{1y}^2$, $\omega^2\mu_0\epsilon_2 = k_z^2 + k_{2y}^2$, and $\omega^2\mu_0\epsilon_3 = k_z^2 + k_{3y}^2$ and

$$\begin{aligned}&\tan\left(\bar{k}_{1y}a\right)/\bar{k}_{1y} + \tan\left[\bar{k}_{2y}(b-a)\right]/\bar{k}_{2y}\\ &\quad + \tan\left[\bar{k}_{3y}(c-b)\right]/\bar{k}_{3y}\\ &= \left(\tan\left(\bar{k}_{1y}a\right)/\bar{k}_{1y}\right)\tan\left[\bar{k}_{2y}(b-a)\right]\bar{k}_{2y}\\ &\quad\cdot\left(\tan\left[\bar{k}_{3y}(c-b)\right]/\bar{k}_{3y}\right)\end{aligned} \tag{4}$$

where $\omega^2\mu_0\epsilon_1 = k_z^2 + \bar{k}_{1y}^2$, $\omega^2\mu_0\epsilon_2 = k_z^2 + \bar{k}_{2y}^2$, and $\omega^2\mu_0\epsilon_3 = k_z^2 + \bar{k}_{3y}^2$. The conductor losses for the TM^{y} mode are

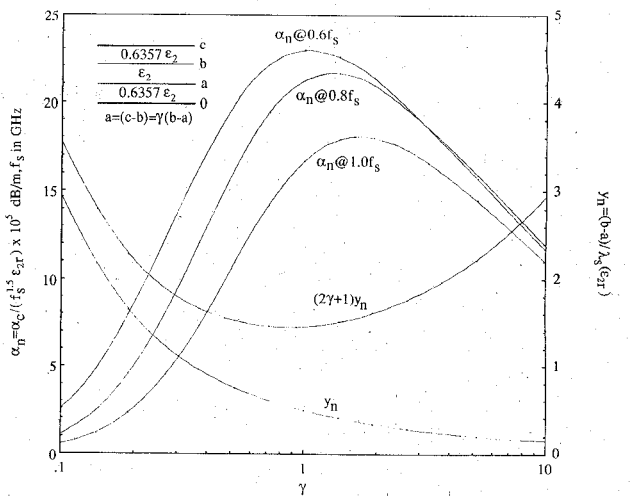

(a)

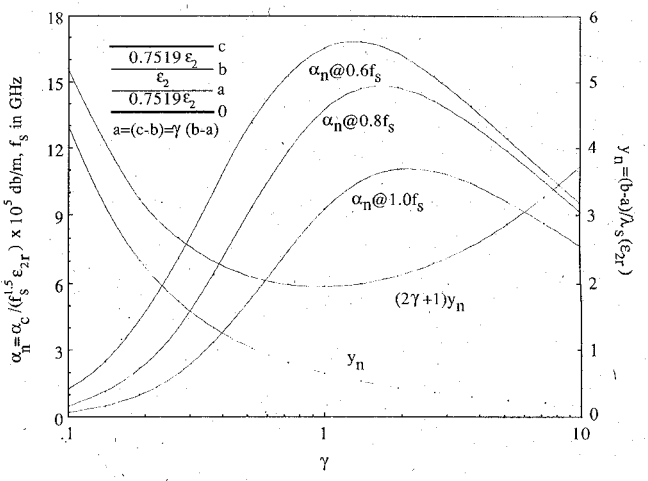

(b)

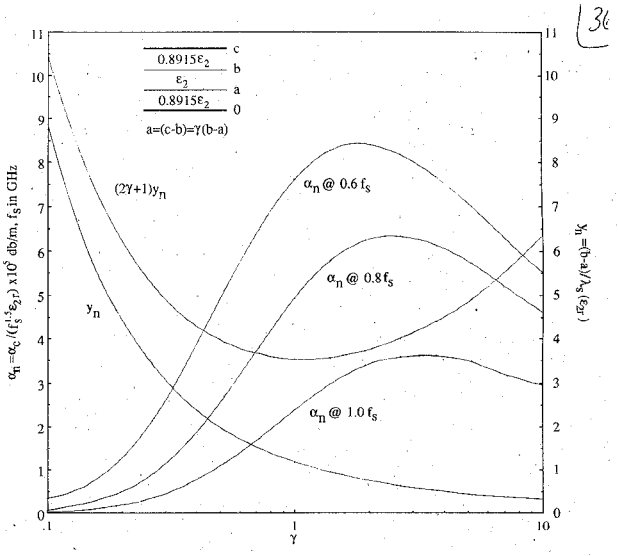

(c)

Fig. 4. Optimized parameters for the parallel-plate waveguide for intersection of the TM^{y} and TE^{y} mode dispersion curves at a frequency f_s. (a) $\epsilon_1 = \epsilon_3 = 0.6357\epsilon_2$. (b) $\epsilon_1 = \epsilon_3 = 0.7519\epsilon_2$. (c) $\epsilon_1 = \epsilon_3 = 0.8915\epsilon_2$.

given by

$$\alpha_c = R_s \int_c |\boldsymbol{H}_t|^2 \, dl \Big/ \left(2 \operatorname{Re} \int_s (\boldsymbol{E} \times \boldsymbol{H}^*) \cdot \hat{z} \, ds \right)$$

$$= \left[\omega R_s / (2k_z) \right] \left[\phi^2(c) + \phi^2(0) \right] \Big/ \int_0^c \phi^2(y) / \epsilon(y) \, dy \quad (5)$$

where $R_s = 2.61 \times 10^{-7} f^{0.5}$ Ω for copper.

To build the parallel-plate design curves, the TM^y and TE^y eigenvalue equations are optimized by varying the structure dimensions to provide for dispersion curve intersection at a given f_s. The structure is symmetric with $a = (c - b) = \gamma(b - a)$ and $\epsilon_1 = \epsilon_3$, where γ is the dimensionless optimization variable. The resulting curves of Fig. 4 plot the proper structure dimensions (normalized as y_n) to achieve intersection at f_s and the conductor losses for copper at $0.6f_s$, $0.8f_s$, and $1.0f_s$ as a function of γ.

Several observations can be made concerning the plots. The dominant features are a minimum in the overall structure size [since $c = (2\gamma + 1) \times (b - a)$], a peak in the conductor loss, and increasing conductor loss with decreasing frequency (an intuitive result). These features contradict, resulting in design tradeoffs between loss and size, and loss and higher order modes. Additionally, the magnitude of the dielectric constant step ϵ_2/ϵ_1 (see Fig. 2) affects the loss. For a given structure size, the loss decreases as the step increases; however, smaller steps, with the resulting larger structures, result in smaller losses.

III. Mode-Matching Analysis

The mode-matching procedure used is an extension of the method used by Mittra *et al.* [11] to include the bifurcation introduced by the center strip metallization. The method is applied to the generalized microstrip problem shown in Fig. 5 in order to simplify the formulation. The Microslab problem is then solved as a specific implementation.

The generalized microstrip structure can be modified to simplify the formulation. Lateral symmetry is exploited to divide the structure along the $x = 0$ plane, thereby reducing the problem by half. A magnetic wall at the $x = 0$ plane eliminates the odd modes, while an electric wall eliminates the even modes. The resulting structure is subdivided for modal expansion as shown in Fig. 6. Note that the formulation process below $y = c$ is identical to that above. The formulation details for both areas are available in [11]. We will outline the steps in order to include the material relevant to the solution of the generalized microstrip.

The method is based on the expansion of the fields in each region in their most general form. For this problem, each region is a truncated section of parallel-plate waveguide, the modal solution of which can be found through the solution of (1) and (2), with $\theta(x)$ and $\bar{\theta}(x)$ taking a general sinusoidal or decaying exponential form. The general field in each region is then an infinite expansion of the modal solutions for its corresponding parallel-plate waveguide. For computer implementation, the expansions are

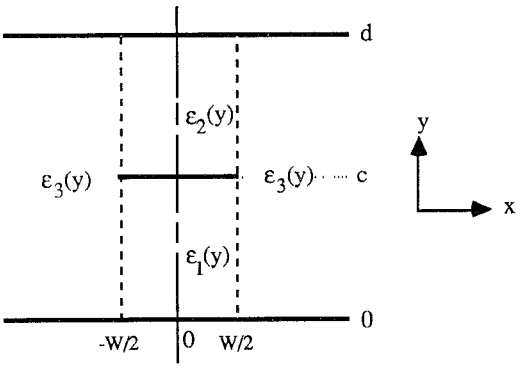

Fig. 5. Generalized microstrip.

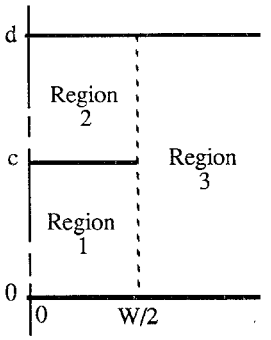

Fig. 6. Subdivision for analysis.

truncated at M, N, and L terms in regions 1, 2, and 3, respectively. We retain an equal number of TM^y and TE^y modes so that the total number of terms in each region is $2M$, $2N$, and $2L$. The boundary conditions at the interfaces between the regions are then matched. Orthogonality is applied to solve for the expansion coefficients in regions 1 and 2 using the relations

$$\int_0^c \phi_{1m}(y) \phi_{1n}(y) / \epsilon_1(y) \, dy = 0, \qquad m \neq n \quad (6a)$$

$$\int_0^c \bar{\phi}_{1m}(y) \bar{\phi}_{1n}(y) \, dy = 0, \qquad m \neq n \quad (6b)$$

$$\int_c^d \phi_{2m}(y) \phi_{2n}(y) / \epsilon_2(y) \, dy = 0, \qquad m \neq n \quad (6c)$$

$$\int_c^d \bar{\phi}_{2m}(y) \bar{\phi}_{2n}(y) \, dy = 0, \qquad m \neq n \quad (6d)$$

where the subscripts refer to the region of application. The expansion coefficients in regions 1 and 2 are eliminated to yield two sets of homogeneous equations for the expansion coefficients in region 3, which must be solved simultaneously. The eigenvalues (propagation constants) of this system are found by forcing the determinant of this system to vanish. The expansion coefficients in region 3 are then found by choosing one arbitrarily and then solving the resulting least-squares problem using the QR factorization. The coefficients in regions 1 and 2 can then easily be computed.

The remaining implementation details concern the number of retained expansion terms, the dielectric composition of each region, and the variable type used in the computa-

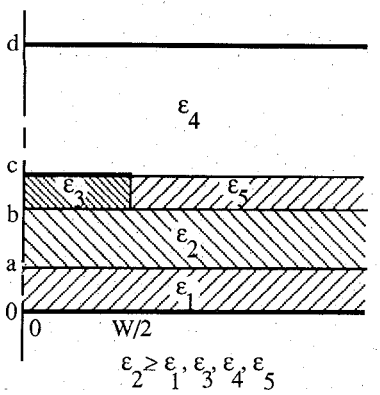

Fig. 7. Dielectrics used in implemented solution.

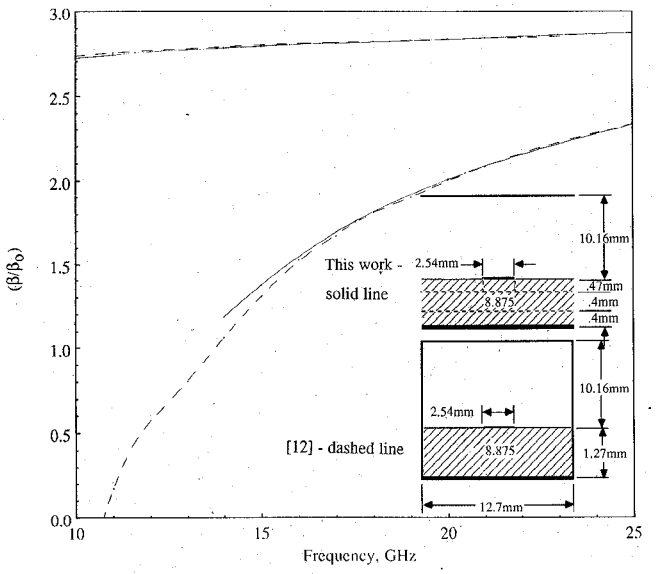

Fig. 8. Microstrip dispersion results.

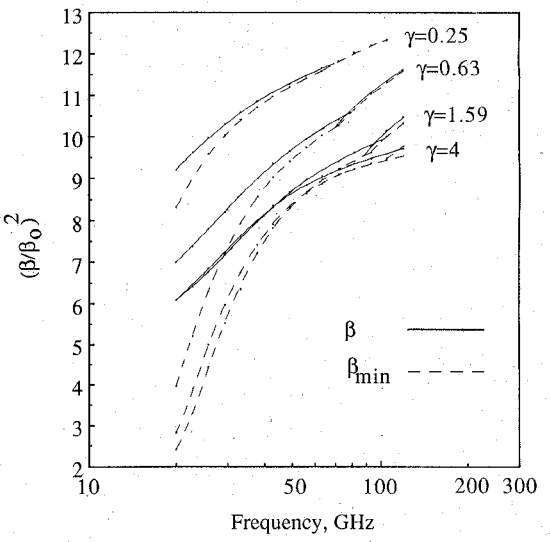

(a)

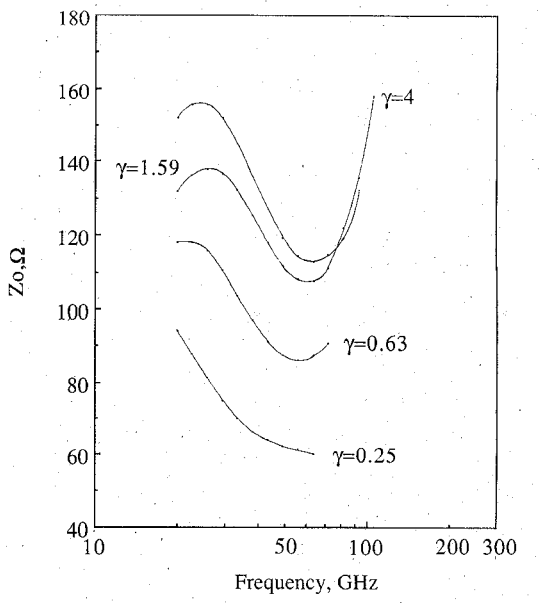

(b)

Fig. 9. Microslab results for several γ. (a) Dispersion. (b) Characteristic impedance.

tion. There are two requirements on the number of expansion terms retained: a square matrix requires that $M+N=L$, and matching the spectral components along the regional interface requires that $M/N=c/(d-c)$. The number of modes in one region is chosen to select the accuracy of the solution. The specific dielectrics implemented are shown in Fig. 7, where the ϵ_5 dielectric layer was added to the basic Microslab structure to facilitate checking the program. Finally, the problem is formulated entirely in real functions, and only real solutions are searched and computed. This limits the search to nonleaky solutions (of primary interest), but it greatly reduces the computation time.

The program was checked by computing the dispersion curve for a covered microstrip line. The results appear in Fig. 8 along with the results of Yamashita *et al.* [12] for an enclosed microstrip line. The two sets of curves agree quite well except at low frequencies, where the side walls influence the results from [12].

The definition implemented for the characteristic impedance calculation is dictated by the behavior of the current on the center strip metallization. Since the fields connect with the strip metallization via evanescent fields, the induced current is small. As the frequency increases, the fields decay more rapidly and even smaller currents are produced. As $f\to\infty$, then $I\to 0$. Consequently, $Z_0=P/(II^*)\to\infty$ and $Z_0=V/I\to\infty$. This undesirable behavior is not found in the power–voltage definition; therefore, it will be used here. The integration path for the voltage is taken from 0 to c along $x=0$ in Fig. 5.

IV. Design Tradeoffs

This section investigates Microslab operation so that a set of guidelines for the design of Microslab can be determined. The parallel-plate analysis of Section II provides guidelines for selecting structure dimensions as a function of γ (see Fig. 4). In this section, the effect of γ on Microslab operation is investigated.

TABLE I
MICROSLAB DESIGN TRADEOFFS

Characteristic	Decreasing $\gamma < \gamma_0$	Increasing $\gamma > \gamma_0$
Dispersion	decreases	decreases
Decay rate	decreases	decreases
Impedance	improves	worsens
Higher order modes	increases	decreases
Size	increases	increases
Loss	decreases	increases†

† Increases over the range of interest.

Several microslab structures were designed using the chart in Fig. 4(b) with γ values of 0.25, 0.63, 1.59, and 4. The structures were analyzed with the mode-matching analysis of Section III, and since exact answers were not required, we chose $d = 2c$ and $M = 6$. For all cases, we chose $w = c/2$ in order to obtain similar modes of operation. The dispersion and impedance curves appear in Fig. 9. Modes with effective dielectric constants at and below the dashed curve, labeled $\beta_{\min}$, are leaky. From this figure and the discussion in Section II on parallel-plate waveguide tradeoffs, the design tradeoffs in Table I are deduced. In this table, γ_0 is defined as the γ for which the minimum structure size is realized.

V. DESIGN CHARTS

Design charts for the propagation constant and characteristic impedance of Microslab lines on GaAs substrates are presented in this section. The dimensions were chosen from the charts in Fig. 4 and the tradeoffs in Table I. Three specific implementations corresponding to the three charts in Fig. 4 are presented in Figs. 10, 11, and 12. The dispersion curves are plotted only where a single nonleaky mode exists. Below the dashed line, leaky modes may exist. The computations were spread among two computers. Each design chart data point for both the propagation constant and impedance calculations required approximately 1.5 min on a VAX 11/780 or 2.2 sec on a Cray X-MP 24. A representative set of field plots for the case $\epsilon_1 = \epsilon_3 = 9.7$ (Fig. 11) is given in Fig. 13, where the fields are reduced by the scale factor given in each plot. The vectors show the field value at the tail. Note that $g = w/2$ and that the longitudinal vectors in (b) and (d) are rotated into the page and plotted at an arbitrary angle.

The convergence criterion is of considerable importance. Included with each design chart is the convergence curve for the number of modes used in the solution. Convergence tests are performed for a narrow strip at the lowest frequency of the design chart, where convergence is slowest. The first solution to fall within ± 0.5 percent in propagation constant and ± 1.5 percent in impedance of the convergent values is accepted. Note that the convergence curves are approximately oscillatory and damped, allowing for the estimation of the convergent value.

The height d selected for the coverplate is also important. Since region 2 of Fig. 6 contains a homogeneous dielectric, the fields in the region will always be sinusoidal in nature. As a result, the plate must be set very high in

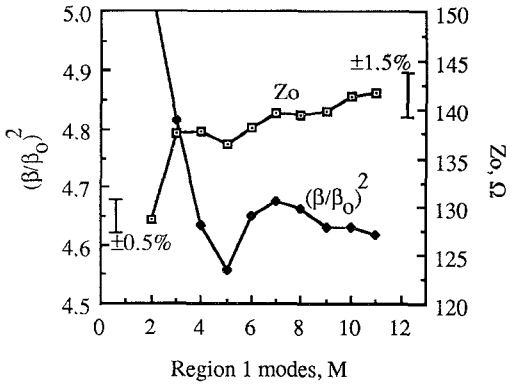

(a)

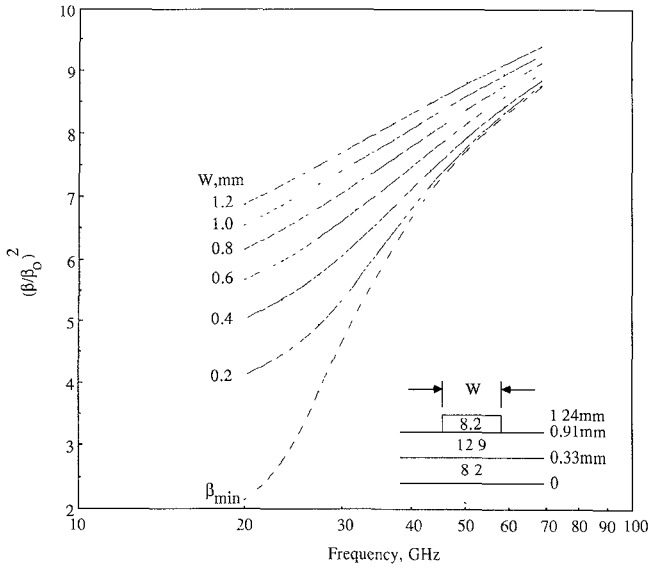

(b)

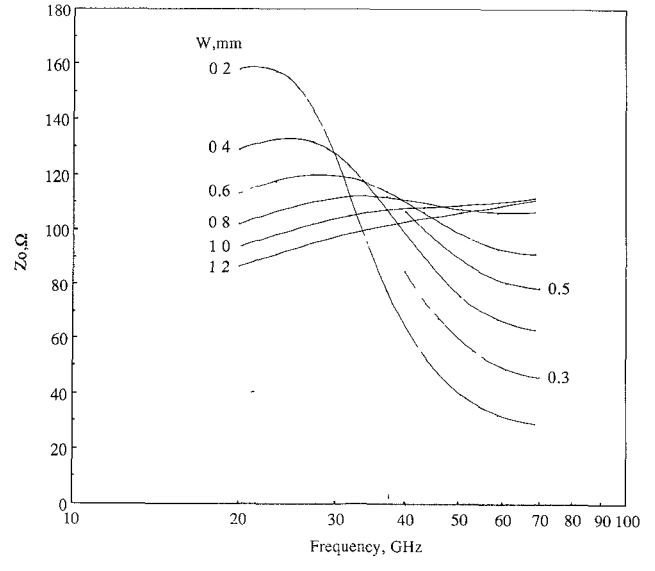

(c)

Fig. 10. Microslab design charts for $\epsilon_{1r} = \epsilon_{3r} = 8.2$ and $\epsilon_{2r} = 12\,9$. (a) Convergence. (b) Dispersion. (c) Characteristic impedance

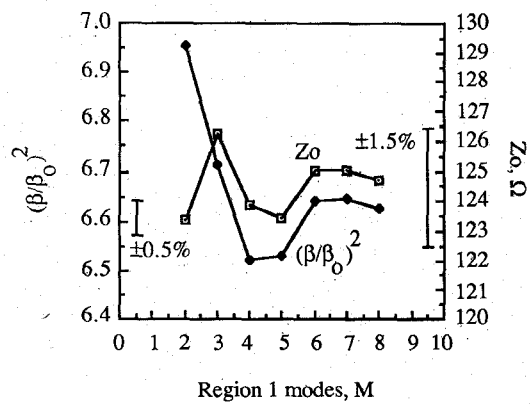

(a)

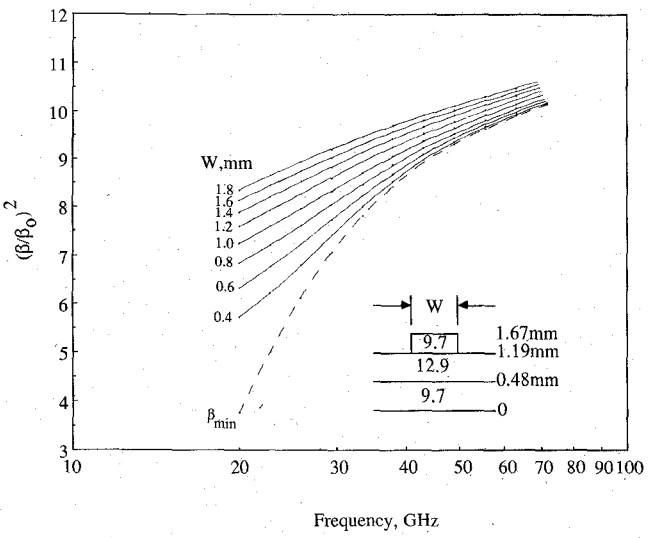

(b)

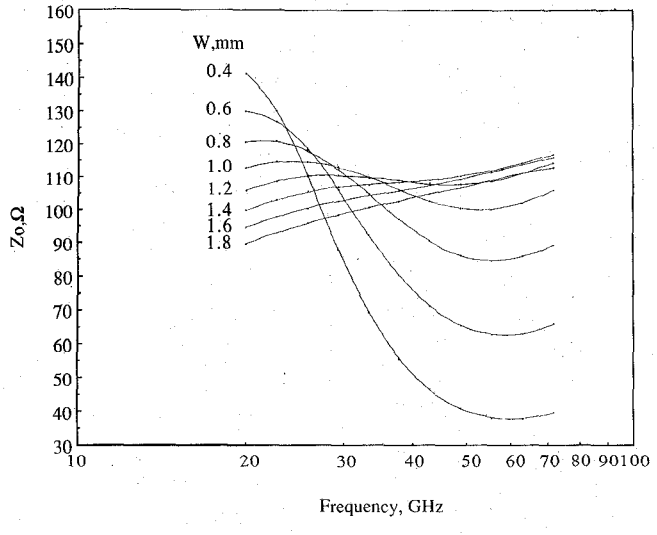

(c)

Fig. 11. Microslab design charts for $\epsilon_{1r} = \epsilon_{3r} = 9.7$ and $\epsilon_{2r} = 12.9$. (a) Convergence. (b) Dispersion. (c) Characteristic impedance.

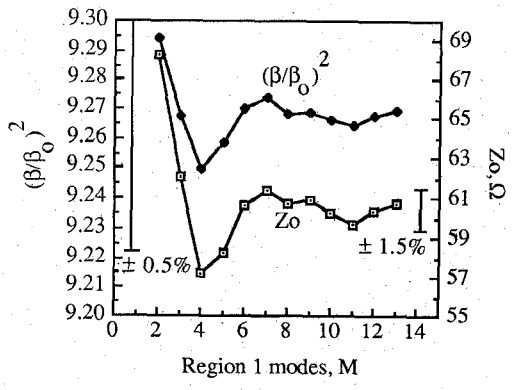

(a)

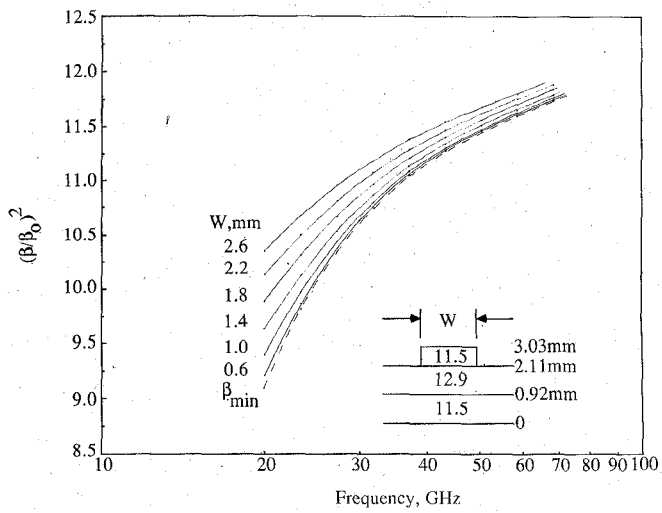

(b)

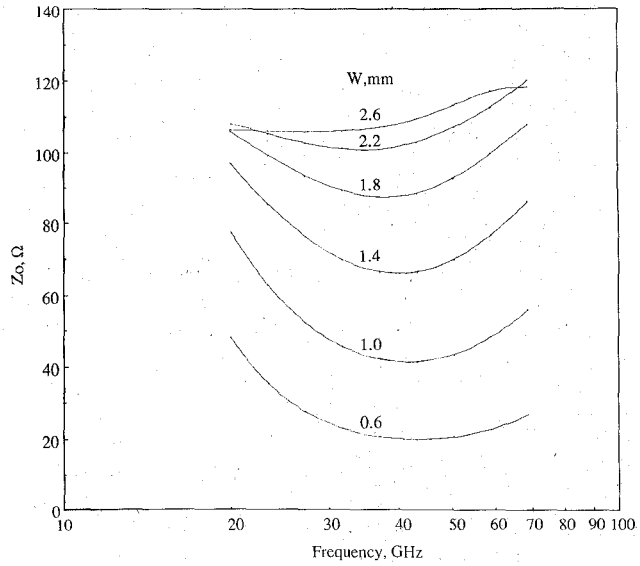

(c)

Fig. 12. Microslab design charts for $\epsilon_{1r} = \epsilon_{3r} = 11.5$ and $\epsilon_{2r} = 12.9$. (a) Convergence. (b) Dispersion. (c) Characteristic impedance.

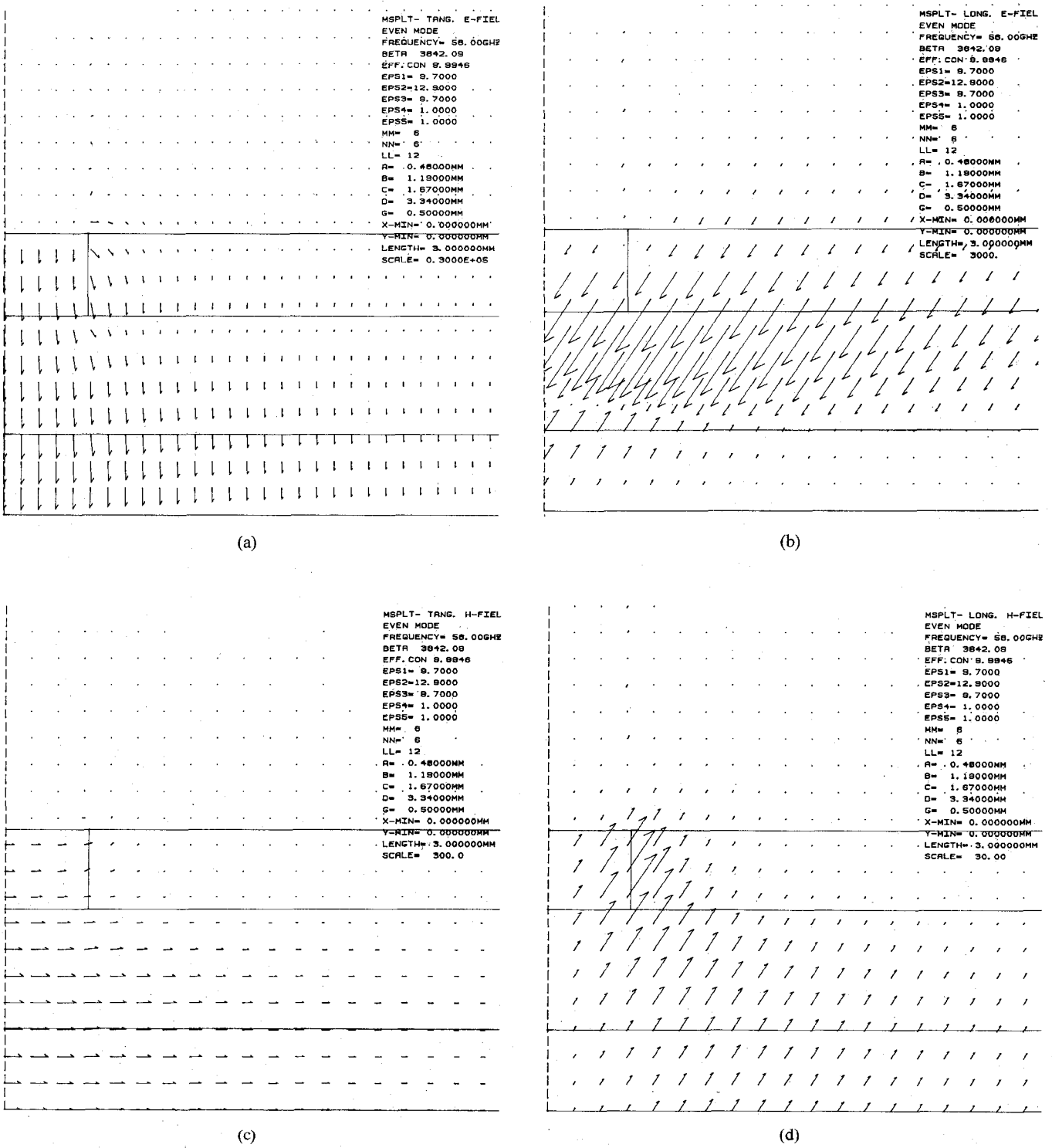

Fig. 13. Field plots for the case $\epsilon_{1r} = \epsilon_{3r} = 9.7$ and $\epsilon_{2r} = 12.9$, $w = 1$ mm. (a) Tangential E field. (b) Longitudinal E field. (c) Tangential H field. (d) Longitudinal H field.

order to approximate an open Microslab. Since the computation time greatly increases as the plate height increases, it is not possible to simulate the open Microslab case. Instead, we place the coverplate at a half free-space wavelength above the center strip metallization at the lowest frequency of the design curve. The plate remains at this height for all frequencies. The plate height is reduced if there is a negligible ($\ll 1$ percent) effect on both the propagation constant and the impedance in order to save on computation time.

The design charts show similar features. The dispersion curves demonstrate the expected behavior where the effective dielectric constant increases with increasing width. The impedance curves are more complicated. At low frequencies, the fields penetrate the insulating dielectrics and Microslab behaves like microstrip: impedance increases

with frequency and decreases with strip width. At high frequencies, the fields do not penetrate the insulating dielectrics as well, and the impedance exhibits behavior derived from both microstrip and dielectric slab operation. The resulting behavior is unintuitive and quite complex.

VI. Conclusions

Microslab waveguide was analyzed in an approximate manner using the parallel-plate waveguide as a model and then accurately using a mode-matching procedure. Use of the model allowed optimization to be performed, which would not have been possible using mode matching alone. The results are design charts where the loss has been minimized in an approximate manner. Experimental verification of the charts is still required.

References

[1] H. B. Sequeira and J. A. McClintock, "Microslab™—A novel planar waveguide for mm-wave frequencies," in *5th Benjamin Franklin Symp. Dig.* (Philadelphia, PA), May 4, 1985, pp. 67–69.

[2] W. V. McLevige, T. Ioth, and R. Mittra, "New waveguide structures for millimeter-wave and optical integrated structures," *IEEE Trans. Microwave Theory Tech.*, vol. MTT-28, pp. 788–794, Oct. 1975.

[3] T. Itoh, "Inverted strip dielectric waveguide for millimeter-wave integrated circuits," *IEEE Trans. Microwave Theory Tech.*, vol. MTT-24, pp. 921–927, Nov. 1976.

[4] R. A. Pucel, D. J. Masse, and C. P. Hartwig, "Losses in microstrip," *IEEE Trans. Microwave Theory Tech.*, vol. MTT-16, pp. 342–350, June 1968.

[5] H. B. Sequeira, J. A. McClintock, B. Young, and T. Ioth, "A millimeter-wave Microslab™ oscillator," *IEEE Trans. Microwave Theory Tech.*, vol. MTT-34, pp. 1333–1336, Dec. 1986.

[6] R. Pregla, "Determination of conductor losses in planar waveguide structures," *IEEE Trans. Microwave Theory Tech.*, vol. MTT-28, pp. 433–434, April 1980.

[7] K. Bierwirth, N. Schulz, and F. Arndt, "Finite-difference analysis of rectangular dielectric waveguide structures," *IEEE Trans. Microwave Theory Tech.*, vol. MTT-34, pp. 1104–1114, Nov. 1986.

[8] U. Crombach, "Analysis of single and coupled rectangular dielectric waveguides," *IEEE Trans. Microwave Theory Tech.*, vol. MTT-29, pp. 870–874, Sept. 1981.

[9] S. Ramo, J. Whinnery, and T. Van Duzer, *Fields and Waves in Communication Electronics*. New York: Wiley, 1984, p. 752.

[10] R. F. Harrington, *Time-Harmonic Electromagnetic Fields*. New York: McGraw-Hill, 1961, p. 129.

[11] R. Mittra, Y. Hou, and V. Jamnejad, "Analysis of open dielectric waveguides using mode-matching technique and variational methods," *IEEE Trans. Microwave Theory Tech.*, vol. MTT-28, pp. 36–43, Jan. 1980.

[12] E. Yamashita and K. Atsuki, "Analysis of microstrip-like transmission lines by nonuniform discretization of integral equations," *IEEE Trans. Microwave Theory Tech.*, vol. MTT-24, pp. 195–200, Apr. 1976.

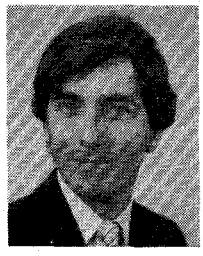

Brian Young was born in Dallas, TX, on November 21, 1961. He received the B.S.E.E. degree (with honors) in 1984 from Texas A&M University and the M.S.E.E. degree in 1985 from the University of Illinois, where he was a research assistant in the Ionosphere Radio Research Laboratory. He is currently working towards the Ph.D. degree at the University of Texas at Austin while working as a research assistant in microwave field theory. Mr. Young was a GTE Fellow for 1985–86. His research interests include electromagnetic theory, numerical electromagnetics, and microwave CAD.

Tatsuo Itoh (S'69–M'69–SM'74–F'82) received the Ph.D. degree in electrical engineering from the University of Illinois, Urbana, in 1969.

From September 1966 to April 1976, he was with the Electrical Engineering Department, University of Illinois. From April 1976 to August 1977, he was a Senior Research Engineer in the Radio Physics Laboratory, SRI International, Menlo Park, CA. From August 1977 to June 1978, he was an Associate Professor at the University of Kentucky, Lexington. In July 1978, he joined the faculty at the University of Texas at Austin, where he is now a Professor of Electrical and Computer Engineering and Director of the Electrical Engineering Research Laboratory. During the summer of 1979, he was a guest researcher at AEG-Telefunken, Ulm, West Germany. Since September 1983, he has held the Hayden Head Centennial Professorship of Engineering at the University of Texas. In September 1984, he was appointed Associate Chairman for Research and Planning of the Electrical and Computer Engineering Department.

Dr. Itoh is a member of the Institute of Electronics and Communication Engineers of Japan, Sigma Xi, and Commissions B and D of USNC/URSI. He served as the Editor of the IEEE Transactions on Microwave Theory and Techniques for 1983–1985. He serves on the Administrative Committee of the IEEE Microwave Theory and Techniques Society. Dr. Itoh is a Professional Engineer registered in the state of Texas.